



### **Science Arts & Métiers (SAM)**

is an open access repository that collects the work of Arts et Métiers Institute of Technology researchers and makes it freely available over the web where possible.

This is an author-deposited version published in: <https://sam.ensam.eu>  
Handle ID: <http://hdl.handle.net/10985/8547>

#### **To cite this version :**

Thanh Hung NGUYEN, Betty LEMAIRE-SEMAIL, Gabriel ABBA, Christophe GIRAUD-AUDINE -  
Modelling of forging processes assisted by piezoelectric actuators : principles and experimental  
validation - IEEE Transactions on Industry Applications - Vol. 50, n°1, p.244-252 - 2014

Any correspondence concerning this service should be sent to the repository

Administrator : [scienceouverte@ensam.eu](mailto:scienceouverte@ensam.eu)



# Modelling of forging processes assisted by piezoelectric actuators : principles and experimental validation

T. H. Nguyen, C. Giraud-Audine, B. Lemaire-Semail, G. Abba, R. Bigot

**Abstract**—This paper presents the modelling of a forging processes assisted by a piezoelectric actuator (PA), which is used to generate specific low frequency vibration waveforms. Experimental results show that such waveforms reduce the necessary forging force during upsetting tests. The main problems which remain are defining the appropriate waveforms, predicting their influence on the process and the actuator and designing the control. Due to the complexity of the interactions between the different components of the system, a complete model of the process is needed. Such a model is developed here using an energetic macroscopic representation to preserve causality throughout the modelling. Simulation results are then compared to representative experimental results.

**Index Terms**—Energetic Macroscopic Representation, Forging, Graphical models, Modelling, Piezoelectric actuator

## I. NOMENCLATURE

Displacement	$q$	[m]
Force generated by PA	$F$	[N]
Piezoelectric force	$F_C$	[N]
Elastic force	$F_S$	[N]
Forging load	$F_M$	[N]
Electrical charge	$Q$	[C]
Voltage	$U$	[V]
Current entering the actuator	$i$	[A]
Motional current	$i_C$	[A]
Stiffness of PA	$K_S$	$[\frac{N}{m}]$
Electromechanical conversion factor	$K_C$	$[\frac{C}{m}]$
Electrical capacitor of PA	$C$	[F]
External radius of workpiece	$r_e$	[m]
Height of workpiece	$h$	[m]
Coulomb coefficient	$\mu$	[-]
Flow stress	$\sigma_0$	[Pa]
Material yield stress	$\sigma_y$	[Pa]
Hardening stress	$\sigma_H$	[Pa]
Viscous stress	$\sigma_v$	[Pa]
Material strain	$\varepsilon$	[-]
Material strain in plastic domain	$\varepsilon_p$	[-]
Material strain in elastic domain	$\varepsilon_e$	[-]
Young's modulus	$E$	[Pa]
Hardening modulus	$H$	[Pa]
Dynamical viscous coefficient	$\eta$	[Pa.s]

T. H. Nguyen, Ch. Giraud-Audine, B. Lemaire-Semail are with Laboratoire d'Electrotechnique et d'Electronique de Puissance de Lille (L2EP), Université des Sciences et Technologies de Lille (USTL), Villeneuve d'Ascq, France (email: thanh-hung.nguyen@ensam.eu)

G. Abba, R. Bigot are with Laboratoire de Conception, Fabrication et Commande (LCFC), École Nationale Supérieure d'Arts et Métiers de Metz, Metz, France (email: gabriel.abba@ensam.eu)

## II. INTRODUCTION

During the last few decades, the use of vibrations in forming processes has caught the attention of different researchers. Such vibrations, superimposed to the normal movement of the die, cause some reduction of the required force. In the seminal experiment published by Blaha [1], ultrasonic sinusoidal vibrations (10-15 kHz) were applied by a Langevin resonator to a zinc specimen during a tensile test. The results are presented on Fig.(1).

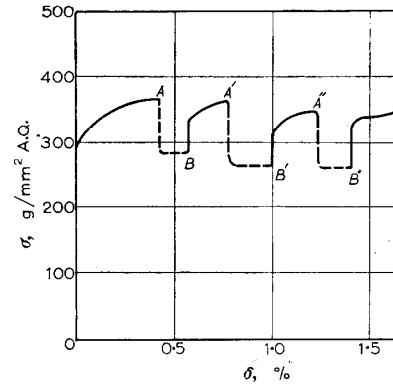


Fig. 1. Stress-strain curve of zinc crystals under ultrasonic action [1]

Since then, other researchers have reproduced this phenomenon on different forming processes. Along with the reduction of the mean processing effort, vibrations have been reported to have other beneficial effects, such as the improvement of the surface's quality. The effect of ultrasonically oscillating dies in longitudinal mode studied on wire drawing by Siegert and Möck [2] and then on tube drawing by Siegert and Ulmer [3] gives the reduction of drawing force in function of the amplitude and the improvement of surface's quality. Later, Marakawa et al. [4] found the deformation resistance of the stainless steel wire reduced and the wiring performance improved when the ultrasonic vibrations is applied to the die radially. In the extrusion process, Mousavi et al. [5] investigated the effects of extrusion speeds, vibration amplitude, vibration frequency and frictional conditions on the extrusion force by using the finite element method. Recently, the press forming is also surveyed by both of numerical simulation and experiment by Ashida et al. [6]. In this study, the wrinkling and cracking phenomenon is avoided due to the use of ultrasonic vibrations. Another recent research by Huang et al. [7]–[10] on the compression tests of plasticine and aluminium specimens reported the force's reduction during the application of ultrasonic vibrations. This phenomenon also gives the similar effect in the microforming [11]. The

studies of using ultrasonic vibrations in micro-extrusion [12], micro-upsetting [13] show a significant load's reduction and substantial improvement in the surface of the microforming parts.

The experiments or simulations presented in the previous works were conducted with ultrasonic sinusoidal vibrations. However, recent results seem to indicate that low frequency waveforms and low amplitude can have a similar effect [14]–[16]. This observation is important as it means that a wider range of waveforms can be used. This also indicate that the power requirement are modest. In this case, the Langevin resonator is not necessary any more and as a consequence, a broader bandwidth is possible. The requirement for the vibrating assistance are therefore low frequencies, high forces and low power, where piezoelectric stack actuators are a good solution. They also have high stiffness and high force by volume unit. It is thus possible to integrate such actuators due to their compact size.

However, the effectiveness of this effect is affected by many other complicated factors. Izumi et al [17] observed the dependence of the flow stress's reduction on the characteristics of materials and the compression velocity during the compressive deformation of different metals superimposed by ultrasonic vibration. The reduction was related to different material's parameters in this survey. Many other researches in numerical and experimental methods [18]–[21] have been carried out to find out the parameter's influence for different processes but a full model for mechanism's explanation has not been achieved.

Moreover, the global energetic reduction of the whole process has not been defined and optimised because of complexity of the interaction between the different components in the process and their own comportments. Mainly, the load is very non-linear due to the plastic behaviour of the workpiece. Therefore, there is a need for simulation of the whole process in order to:

- Evaluate the effects of a specific waveform on the forging force,
- Estimate the effect of vibrations on different materials,
- Study the perturbation of the load on the actuator,
- Design the control for the process,
- Predict the interaction with the power supply,
- Investigate the sophisticated interaction's model between material and environment.

The contribution of this paper is to propose a model of the complete forging process using the assistance of vibration, that can be exploited to study the effect of low frequency waveform on the process. The description of the process is exposed in the first section. The second part deals with the modelling principles that will be explained and then applied to the different parts of the system. Some simulation results and comparison with experimental results are presented in the third part.

### III. EXPERIMENTAL SYSTEM

#### A. Experiment setup

The process studied is the upsetting of a cylindrical workpiece. Fig.10 shows the experimental equipment used for the test that will be compared to the simulation results. A workpiece is placed between two dies fixed to the machine. The upper die is assumed to move down at constant speed,

while the lower die is animated by periodic vibration due to a device integrating a PA. Since the two steel dies are assumed to be rigid, the relative displacements of the two workpiece surfaces are calculated from the displacements of the two dies, which are measured by displacement sensors. The force generated by the PA is measured by a force sensor between the lower die and the vibrating device. The measured signals of voltage, current and force are passed through a 4<sup>th</sup> order 1 kHz-anti-aliasing filter before being sampled by an acquisition card at 2 kHz, which is synchronised with the counter card that acquires the displacement measurements.

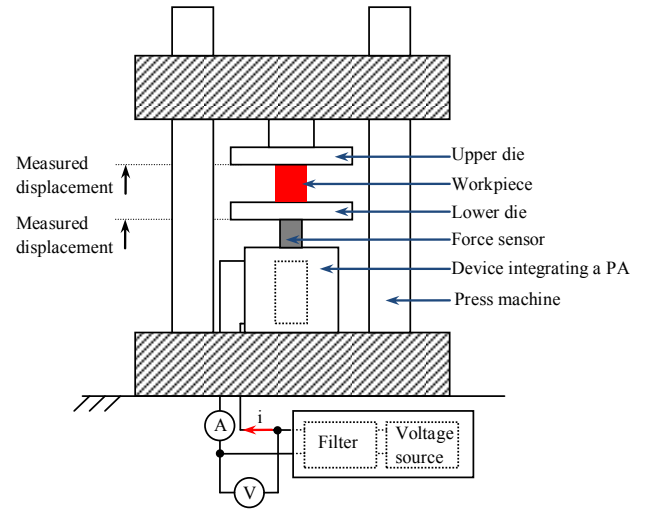


Fig. 2. Experimental setup

The specific elements of equipment are listed in table I.

TABLE I  
EXPERIMENTAL EQUIPMENTS

Displacement sensor	Heidenhain MT2581
Counter card	Heidenhain IK220
Force sensor	Kistler 9351B
Charge amplifier	Kistler 5015A
Current sensor	LEM PR30
Voltage sensor	LEM
Piezoelectric actuator	Piezomechanik Pst1000/16/60
Acquisition card	NI 6124

#### B. Vibrating device

To ensure that the force applied to the PA (1) during the process is only on its longitudinal axis, a vibrating device is designed as in Fig.3. This aim is achieved by using a punctual contact (6) in order to transfer the vibrations from the PA to the plate (5), which is in contact with the force sensor. A cylinder (2) is fastened to the plate to create a linear slide for the punctual contact. The movement of this cylinder is guided by the flexible linkages (4) connected to the outer fixed cylinder (3).

#### C. Power supply

The voltage inverter is used in this dynamic application due to its fast response and high accuracy for the AC supply [22]. Moreover, the use of current control technique for this solution is also an advantage to drive a PA because of its nature as a capacity load. The scheme of power supply

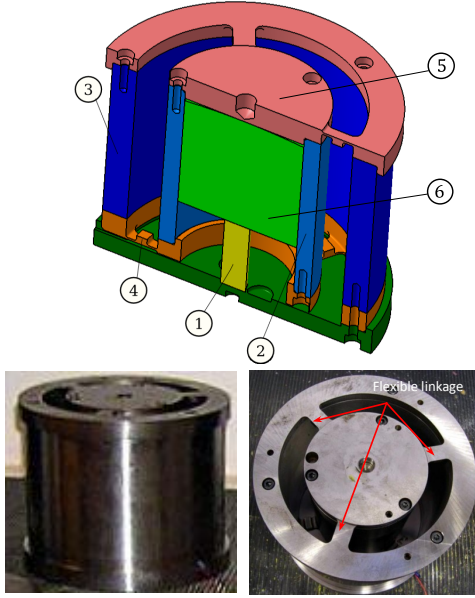


Fig. 3. Device integrating a PA

circuit for the PA is presented in the Fig. 4. The input voltage is connected to the branch U of the voltage inverter through an inductor 100 mH. By using Pulse Width Modulation (PWM) method at 3 kHz with a pre-defined duty cycle, the output voltage is modulated to the required waveform voltage for the PA, which is connected in series with an inductor 10 mH in the branch V.

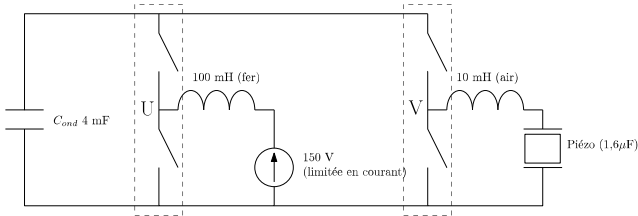


Fig. 4. Power supply's scheme

The values of waveform and the duty cycle used in the voltage inverter are calculated and generated by a computer. These values are then transferred into a digital signal processor through an interface RS232. The PWM function in this processor will automatically generate the required controlling signal for the voltage inverter. These equipments are shown in the Fig.5.

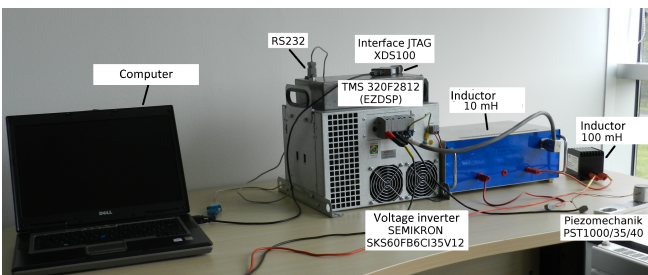


Fig. 5. Electrical equipments

#### IV. MODELLING

In order to carry out the modelling, the Energetic Macroscopic Representation (EMR) [23] developed by the Laboratory of Electrical Engineering and Power Electronics (L2EP-France) is a helpful tool for visualizing causality and clearly understanding the power flows inside the system from the source to dissipating system through power variables. EMR takes no assumptions from mathematical systems into account but concentrates solely on power conversion by using a limited set of symbolic representations (power sources, storage, conversion and coupling, presented in Appendix VII) to highlight the system's energetic properties. Since the nature of each block imposes what can be applied (action) and how the block responds (reaction), causality is revealed naturally throughout the modelling process. Moreover, it gives an easy and solid method of designing the control.

The objective of this section is to model the whole system in order to study the feasibility of using the waveforms and to evaluate their influence on the workpiece's reaction force during the process. The system's modelling is achieved by the symbolic representations of the piezoelectric actuator and workpiece presented in the following parts.

##### A. Energetic Macroscopic Representation of a piezoelectric actuator

At this stage of the study, a sophisticated model of the piezoelectric is not required. In order to describe the actuator's comportment, the following quasi-static equations, widely used by most commercial PA suppliers, are applied in this model:

$$Q = K_C \cdot q + C \cdot U \quad (1)$$

$$F = K_S \cdot q + K_C \cdot U \quad (2)$$

Considering these equations from the view of physical quantity causality, they can be rewritten in the following natural integral causal forms:

$$\int i dt = K_C \int \dot{q} dt + C \cdot U \quad (3)$$

$$F = K_S \int \dot{q} dt + K_C \cdot U \quad (4)$$

The terms  $K_C \int \dot{q} dt$  in (3) and  $K_C \cdot U$  in (4) express the electromechanical conversion inside the PA. This piezoelectric phenomenon is illustrated by a conversion element (see Appendix VII) with a conversion factor  $K_C$ . The relations between the inputs and outputs are defined as follows:

$$F_C = K_C \cdot U \quad (5)$$

$$i_C = K_C \cdot \dot{q} \quad (6)$$

where  $i_C$  is the motional current, and  $F_C$  is the piezoelectric force.

The mechanical energy generated from this conversion, defined by  $\int F_C \dot{q} dt$ , is stored partly under material's elastic energy, defined by  $\int F_S \dot{q} dt$ , and results partly in the output force  $F$ , defined by  $\int F \dot{q} dt$ . Therefore, this energetic relation can be determined by a coupling element and the force generated by the PA is derived from (2) :

$$F = F_C - F_S \quad (7)$$

where  $F_S = -K_S \int \dot{q} dt$  is elastic force inside the PA, which is represented by a mechanical accumulator.

Besides, the electrical charge  $K_C \cdot \int \dot{q} dt$  generated by the PA contributes partly to the total electrical charge  $Q$ . The output voltage is calculated from (1):

$$U = \frac{1}{C} \int (i - i_C) dt \quad (8)$$

This relation is expressed by an electrical accumulator.

Using the EMR symbols given in Appendix VII, the EMR model of the PA will be constructed step by step from the starting point of the entering variables and exiting variables with all components defined above (see Fig.6).

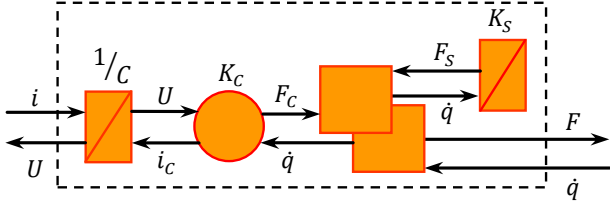


Fig. 6. EMR model for a piezoelectric actuator in the quasi-static mode

### B. Modelling of cylindrical workpiece

The objective of this model is to determine the forging load during the FP. This is achieved using the slab method [24]. Assuming that the material flows radially, the resulting stress field depends solely on the current radius.

In this model, friction is taken into account using the Coulomb model and the sample's geometry is assumed to be conserved during the FP, which means that our sample will retain its cylindrical form. It also means that when the displacement is imposed on the sample by the rigid die, the sliding phenomenon will occur right at the interface during deformation. Writing the equilibrium of slab, the forging load can be obtained by the following equation:

$$F_{fp} = \frac{\pi r_e h}{\mu} \sigma_0 \left( \frac{e^A - 1}{A} - 1 \right) \quad (9)$$

where we introduce  $A = \frac{2\mu r_e}{h}$ . Rewriting this equation as:

$$F_{fp}(t) = \Psi(h(t)) \sigma_0 [\varepsilon(t), \dot{\varepsilon}(t)] \quad (10)$$

reveals that the forging load is equal to the material's flow stress  $\sigma_0$  modulated by the function  $\varepsilon(t) = \frac{\pi r_e h}{\mu} \left( \frac{e^A - 1}{A} - 1 \right)$ , which depends on the Coulomb friction coefficient  $\mu$  and the geometric parameters of the workpiece  $h(t)$  and  $r_e(t)$  (see Fig.7). The latter are imposed by the distance separating the dies  $h(t)$  and the volume conservation of the workpiece.

Therefore, in order to calculate the reaction force, it is essential to estimate the current stress of the cylinder during the FP. This can be accomplished by introducing the constitutive law of the material which relates the flow stress's value to the strain and the strain rate, which are already functions of time:

$$\sigma_0(t) = \sigma_0 [\varepsilon, \dot{\varepsilon}] \quad (11)$$

where  $\varepsilon(t)$  and  $\dot{\varepsilon}(t)$  are imposed by the distance between the dies  $h(t)$  [24]:

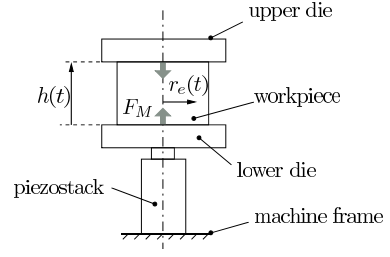


Fig. 7. Schematic of vibration assistance during upsetting of a cylindrical sample

$$\begin{cases} \varepsilon(t) = 1 - \frac{h_0}{h(t)} \\ \dot{\varepsilon}(t) = \frac{d\varepsilon(t)}{dt} \end{cases} \quad (12)$$

Different analytical models can be applied to describe the behaviour of material during the forming process. In the present work, a uni-axial Bingham generalized elasto-viscoplastic model (Fig.8) is applied, as it describes the material behaviours both in the elastic and viscoplastic domains. This is obtained by introducing a slider which imposes  $\dot{\varepsilon}(t) = 0$  as long as  $|\sigma_0(t)| \leq \sigma_y$  where  $\sigma_y$  is the yield stress of the material. In such a case, the material is in the elastic domain and thus behaves like a spring with stiffness  $E$ . Otherwise, plastic flow occurs, and the slider imposes the stress  $\sigma_y$ . The material reacts like a system including a spring in parallel with a viscous damper of damping coefficient  $\eta$  submitted to stress  $\sigma_0(t) - \sigma_y$ .

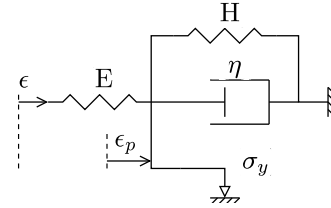


Fig. 8. Bingham's generalized analytical elasto-viscoplastic model

The model's input is the material strain, which is the sum of the elastic strain and the plastic strain:

$$\varepsilon(t) = \varepsilon_p(t) + \varepsilon_e(t) \quad (13)$$

The two states can be discriminated with the help of a control function:

- 1)  $|E \cdot \varepsilon - \sigma_H| < \sigma_y$ : elastic domain which corresponds to the EMR in Fig.9a, where  $\varepsilon_p = 0$  (no plastic flow),
- 2)  $|E \cdot \varepsilon - \sigma_H| > \sigma_y$ : plastic domain, in which the plastic flow appears and the plastic stress  $\sigma_v$  can be determined by:

$$\begin{cases} \sigma_v = \sigma_0 - \sigma_H - \sigma_y & \text{if } E \cdot \varepsilon - \sigma_H > \sigma_y \\ \sigma_v = \sigma_0 - \sigma_H + \sigma_y & \text{if } E \cdot \varepsilon - \sigma_H < -\sigma_y \end{cases} \quad (14)$$

and in this case, the corresponding EMR is presented in Fig.9b.

In Fig.9, two springs in the Bingham model are represented by two mechanical accumulators, where the material elastic energy is acquired during the process; while the two other component including the viscous damper and slider are considered as mechanical sources where energy dissipates.



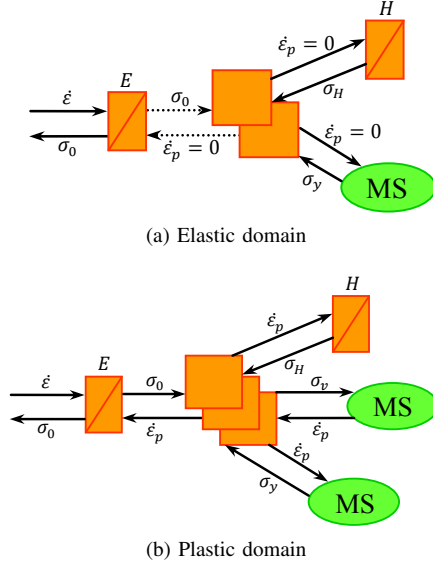


Fig. 9. Material behaviour's EMR

Note that in the current implementation, the non-linear elements for hardening stress and viscous stress were used, namely:

$$\begin{cases} \sigma_v = \eta |\dot{\epsilon}_p|^n \text{sgn}(\dot{\epsilon}_p) \\ \sigma_H = H |\epsilon_p|^m \text{sgn}(\epsilon_p) \end{cases} \quad (m, n > 0) \quad (15)$$

where  $\text{sgn}(\cdot)$  is the sign function.

Parameters  $E, H, \sigma_y, m, n$  are assumed to be constant for a specific material. The solution of equation (14) returns the value of plastic strain  $\epsilon_p$  as a function of the input  $\epsilon$ . The elastic strain  $\epsilon_e$  can then be deduced according to (13).

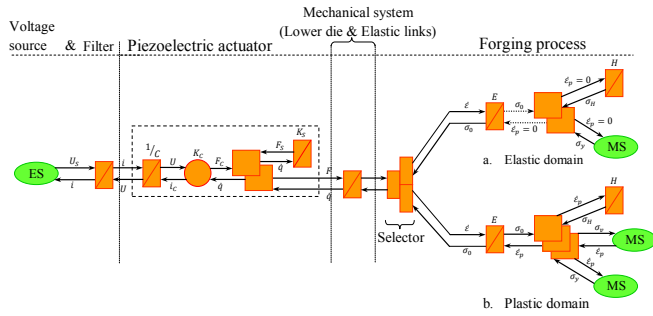


Fig. 10. Complete system's EMR

Finally, the two models described are connected to the model of the mechanical system including the lower die and the elastic links (described in the next section). This electromechanical system is powered by an electrical source through a filter to create a complete model (Fig.10) for the experimental system. Note that the upper die is supposed to be in contact with the workpiece continuously. However, it is the case in practice since the vibrations' amplitude is very small.

## V. RESULTS AND DISCUSSION

### A. Copper specimen

The test was carried out on a Lloyd LR30K material testing machine with a load capacity of 30 kN and a speed range of 0.001 to 508 mm/min.

The workpiece used in this experiment is an annealed copper cylindrical sample geometrically defined in table II. The material parameters provided in this table are identified and validated in other tests with different samples. These values were obtained through previous tests with various waveforms, but the identification procedure is beyond the scope of this paper. The Coulomb friction coefficient  $\mu$  is coarsely estimated. Indeed, a relatively short time at the beginning of the test is considered for the identification. Therefore, the  $A$  term in Eq.9 is almost constant and difficult to identify.

TABLE II  
COPPER SPECIMEN'S PARAMETERS

$h$	7.9	[mm]
$r_e$	6	[mm]
$\sigma_y$	46.7	[MPa]
$E$	22.3	[GPa]
$H$	1.24	[MPa]
$\mu$	1	-
$\eta$	4.83	[GPa.s]
$n$	0.958	-
$m$	0.33	-

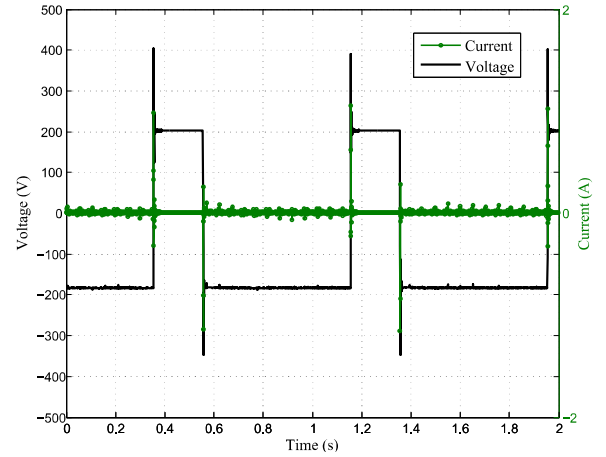


Fig. 11. Inverted output voltage and current in the PA

The voltage is a square wave of duty ratio 10 % with the frequency 1.25 Hz. The peak to peak voltage is 400 V, and the bias voltage of 50 V is superimposed in order to respect the PA voltage rating. A pulsed current with a peak value of 1 A is thus applied to the PA (see Fig.11). The upper die moves down at a speed of 1 mm/min at  $t = 4$  s. The measured displacements and distance variations between the two dies are presented in Fig.12. Results show that the machine is not rigid enough, and in the simulation, the displacement must be adjusted to obtain a displacement of ca. 4  $\mu\text{m}$ .

The measured forging load is compared with the simulated one in Fig.13. First, the simulated variations of the force are of the same magnitude as the measured ones (ca. 250 to 300 N depending on whether the beginning or the end of the curve is considered). However, the oscillations in the simulation are exaggerated, which could be a consequence of the value of  $\eta$  that was identified. As a matter of fact, the waveform used for the identification was triangular, and the speed involved was much lower. It can also be noticed that the initial elasto-plastic transition is a lot faster according to the model. This is known as the limitation of the Bingham model. The results at the end of the test present a departure

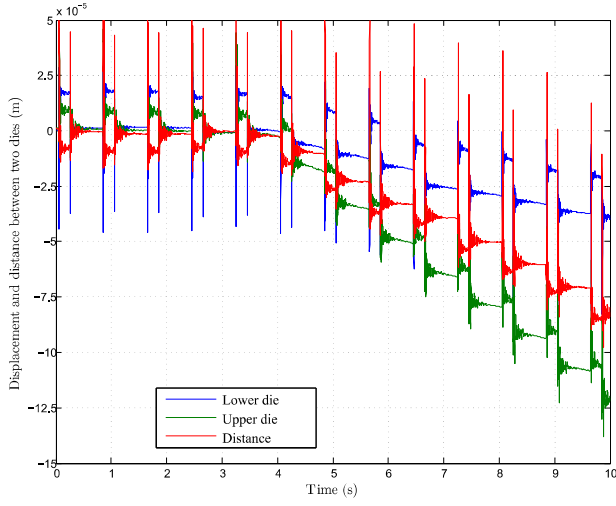


Fig. 12. Displacement and distance's variation between two dies

of the predicted values from the actual ones. This separation can be attributed to the kinematic assumption of the slab model which ignores the barrelling effect common in the upsetting test.

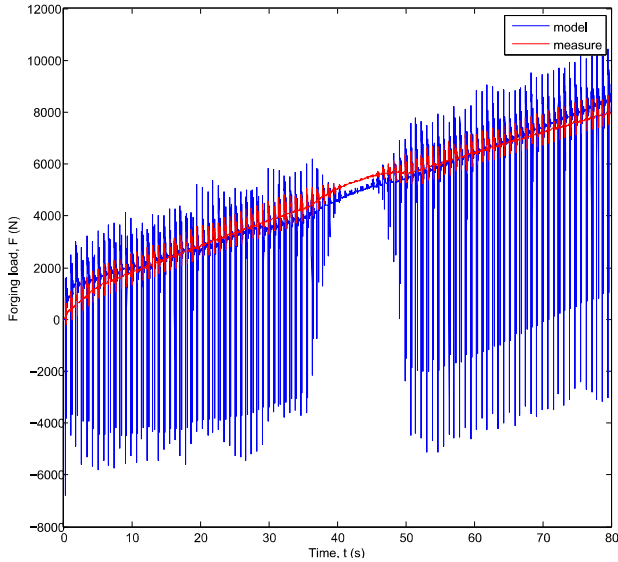


Fig. 13. Measured forging load in comparison with the simulated value in the copper's test

The results are nonetheless encouraging, in particular considering the details visible in Fig.14. The vibration is suppressed around 38 s then put back around 46 s. In both cases this results in an increase of the forging load when the vibration is stopped, then a decrease of the forging load when the vibration is restored. This observation validates the model and the use of vibration. It also offers a practical way to study the influence of the waveforms and their parameters on reducing forging load in future works. Fig.15 gives an example of the influence of the change in waveform amplitude, period, and duty ratio (respectively 6  $\mu\text{m}$ , 50 ms and 40 %) on the forging force.

#### B. Aluminium specimen

The testing machine Zwick/Roell Z1200 with a load capacity of 1200 kN and a speed range of 0.001 to 400 mm/min

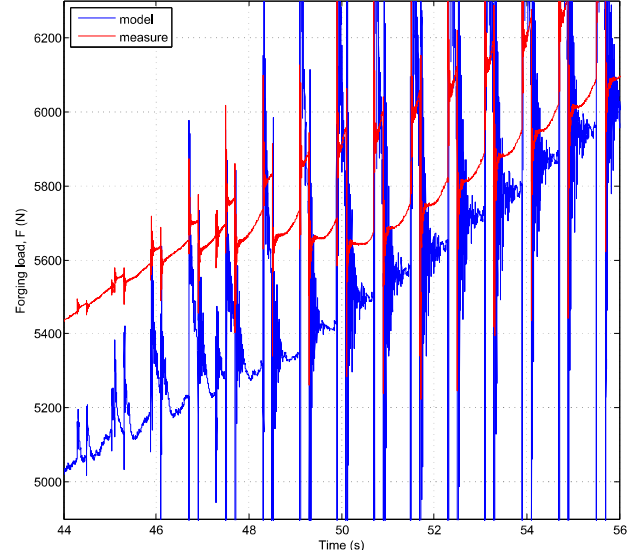


Fig. 14. Detail measured forging load in comparison with the simulated value in the copper's test

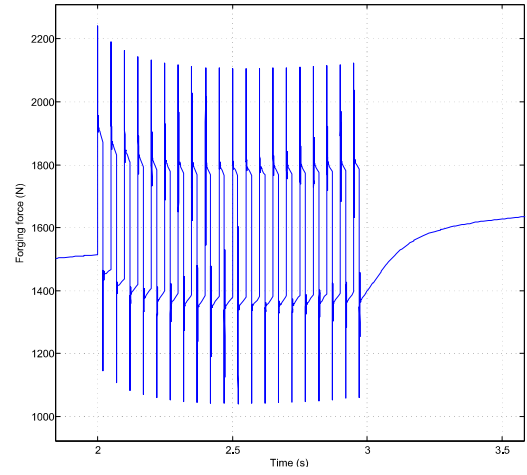


Fig. 15. Influence of waveform parameter change

is used for the test with aluminium specimen. This cylindrical aluminium sample's parameters are defined in table III by a similar identification procedure.

TABLE III  
ALUMINIUM SPECIMEN'S PARAMETERS

$h$	16	[mm]
$r_e$	8	[mm]
$\sigma_y$	58.1	[MPa]
$E$	1.897	[GPa]
$H$	362	[MPa]
$\mu$	1	-
$\eta$	21.3	[GPa.s]
$n$	0.96	-
$m$	0.15	-

The upper die moves down at a speed of 1.5 mm/min. The measured displacements of the two dies are presented in Fig.16. With this larger testing machine, the system's stiffness is significantly improved. Results show the upper die get no influence from the vibrations of the lower die.

The supply voltage in this test is a sinusoidal wave with the voltage peak to peak 550 V and the frequency 2 Hz. The measuring force is presented in the Fig.17 and

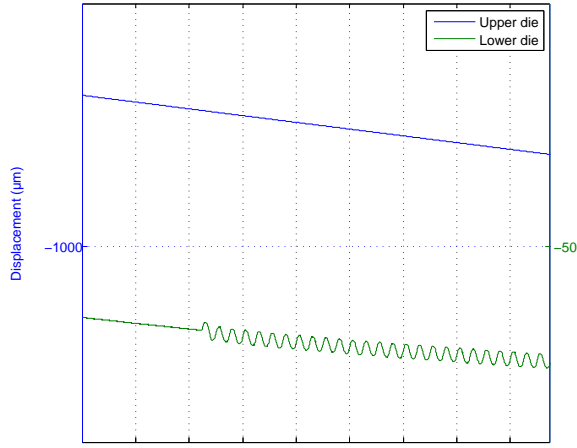


Fig. 16. Two dies' displacement

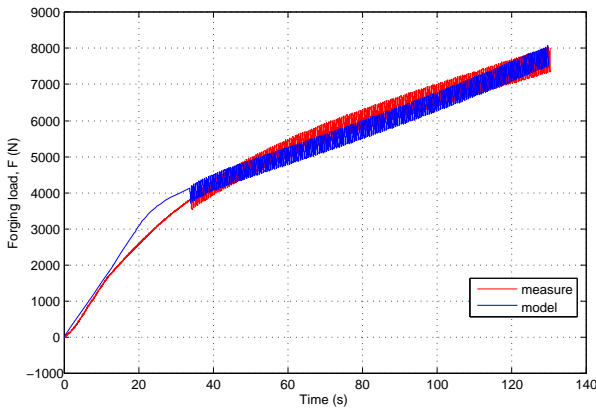


Fig. 17. Measured forging load in comparison with the simulated value in the aluminium's test

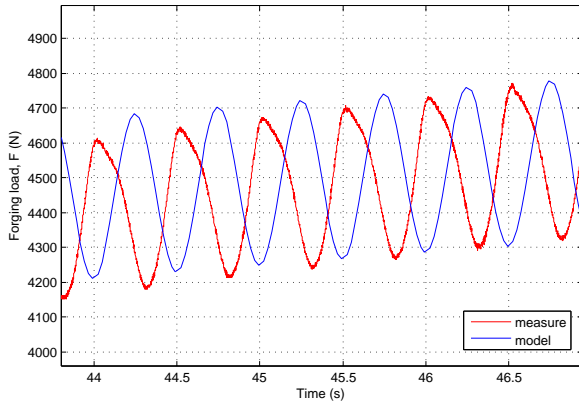


Fig. 18. Detail measured forging load in comparison with the simulated value in the aluminium's test

its detail in the Fig.18. The simulated force shows us the similar effect found in the copper's test. Because of the specimen's imperfectness and the model's limitation, the differences between two results can be found in the elasto-plastic transition and the curve's form. However, the force's variations are found at the same magnitude (ca. 400 N to 550 N). It validates the use of different waveform to reduce the mean force during the forging and the method to predict the influence of vibrations on the different materials.

## VI. CONCLUSION

In this work, the forging process assisted by a piezo-electric actuator in low frequency has been modelled by using Energetic Macroscopic Representation. This model has evaluated approximately the experimental forging load's reduction in the upsetting test with copper and aluminium specimen. The comparison between the simulated and experimental results reveals that the model seems to capture the main features of the process, which could facilitate the study of the impact of different waveforms on forging load. It seems to be a promising tool to study the influence of waveform's parameters on the effectiveness of using vibrations in the forging process.

According to the results obtained, a finer model of material must be achieved to adapt to its sophisticated comportments. The model of the piezoelectric actuator should be also improved. Additionally, the material's parameters must be identified better to have a preciser prediction.

## VII. APPENDIX

### EMR's basic elements

Element	Symbol	Description
Variable	$\begin{array}{c} \xrightarrow{x} \\ \xleftarrow{y} \end{array}$	Action/ reaction variable ( $x/y$ )
Source		Energetic source
Accumulator		Accumulator
Converters		Mono-physic converter
		Multi-physic converter
Couplings		Mono-physic coupling
		Multi-physic coupling

## VIII. ACKNOWLEDGEMENT

The authors would like to thank M. Fendler and Henrion for their technical support during the tests.

## REFERENCES

- [1] F. Blaha and B. Langenecker, "Ultrasonic investigation of the plasticity of metal crystals," *Acta Metallurgica*, vol. 7, no. 2, pp. 93–100, 1959.
- [2] K. Siegert and A. Möck, "Wire drawing with ultrasonically oscillating dies," *Journal of Materials Processing Technology*, vol. 60, pp. 657–660, 1996.
- [3] K. Siegert and J. Ulmer, "Superimposing ultrasonic waves on the dies in tube and wire drawing," *Journal of Engineering Materials and Technology*, vol. 123, oct 2001.
- [4] M. Murakawa and M. Jin, "The utility of radially and ultrasonically vibrated dies in the wire drawing process," *Journal of Materials Processing Technology*, vol. 113, no. 1-3, pp. 81–86, 2001.
- [5] S. Mousavi, H. Feizi, and R. Madoliat, "Investigations on the effects of ultrasonic vibrations in the extrusion process," *Journal of materials processing technology*, vol. 187, pp. 657–661, 2007.
- [6] Y. Ashida and H. Aoyama, "Press forming using ultrasonic vibration," *Journal of Materials Processing Technology*, no. 187-188, pp. 118–122, 2007.
- [7] Z. Huang, M. Lucas, and M. J. Adams, "Influence of ultrasonics on upsetting of a model paste," *Ultrasonics*, vol. 40, pp. 43–48, 2002.



- [8] —, “Modelling wall boundary conditions in an elasto-viscoplastic material forming process,” *Journal of Materials Processing Technology*, no. 107, pp. 267–275, 2000.
- [9] D. Yusof, M. Lucas, and Z. Huang, “Superimposed ultrasonic oscillations in compression tests of aluminium,” *Ultrasonics*, vol. 44, pp. e511–e515, 2006.
- [10] —, “Modelling the effects of superimposed ultrasonic vibrations on tension and compression tests of aluminium,” *Journal of Materials Processing Technology*, vol. 186, pp. 179–190, 2007.
- [11] G. Ngaile and C. Bunget, “Influence of ultrasonic vibration on microforming,” *Transactions of NAMRI/SME*, vol. 36, pp. 137–144, 2008.
- [12] C. Bunget and G. Ngaile, “Influence of ultrasonic vibration on micro-extrusion,” *Ultrasonics*, vol. 51, 2011.
- [13] Z. Yao, G.-Y. Kim, L. Faidley, Q. Zou, D. Mei, and Z. Chen, “Effects of superimposed high-frequency vibration on deformation of aluminum in micro/meso-scale upsetting,” *Journal of Materials Processing Technology*, vol. 212, pp. 640–646, 2012.
- [14] R. Ly, C. Giraud-Audine, G. Abba, and R. Bigot, “Longitudinal vibrations modeling of a piezoelectric actuator used in forming process,” in *Proceedings of the 2009 IEEE International Conference on Mechatronics*, 2009.
- [15] —, “Experimentally validated approach for the simulation of the forging process using mechanical vibration,” *International Journal on Material Forming*, vol. 2, pp. 133–136, 2009.
- [16] A. Khan, C. Giraud-Audine, G. Abba, and R. Bigot, “Effects of vibrations on metal forming process: analytical approach and finite element simulations,” *International Conference on Advances in Materials and Processing Technologies*, 2010.
- [17] O. Izumi, K. Oyama, and Y. Suzuki, “Effects of superimposed ultrasonic vibration on compressive deformation of metals,” *Transactions of the Japan Institute of Metal*, vol. 7, 1966.
- [18] J.-C. Hung and C. Hung, “The influence of ultrasonic-vibration on hot upsetting of aluminum alloy,” *Ultrasonics*, no. 43, p. 692698, 2005.
- [19] J.-C. Hung, Y.-C. Tsai, and C. Hung, “Frictional effect of ultrasonic-vibration on upsetting,” *Ultrasonics*, no. 46, pp. 277–284, 2007.
- [20] J.-C. Hung and C.-C. Lin, “Investigations on the material property changes of ultrasonic-vibration assisted aluminum alloy upsetting,” *Materials and Design*, no. 45, pp. 412–420, 2013.
- [21] M. Hayashi, M. Jin, S. Thipprakmas, M. Murakawa, J.-C. Hung, Y.-C. Tsai, and C.-H. Hung, “Simulation of ultrasonic-vibration drawing using the finite element method (fem),” *Journal of Materials Processing Technology*, no. 140, pp. 30–35, 2003.
- [22] L. Malesani and P. Tomasini, “PWM current control techniques of voltage source converters - a survey,” *Proceedings of the IECON '93, International Conference on Industrial Electronics, Control, and Instrumentation*, nov 1993.
- [23] P. J. Barre, A. Bouscayrol, P. Delarue, E. Dumetz, F. Giraud, J. P. Hautier, X. Kestelyn, B. Lemaire-Semail, and E. Semail, “Inversion based control of electromechanical systems using causal graphical descriptions,” *IEEE-IECON06 (Paris)*, nov 2006.
- [24] K. Lange, *Handbook of metal forming*. McGraw-Hill, 1985.

**Thanh Hung Nguyen** was born in Vietnam in 1983. He received his B.S. degree in Mechatronics from the Ho Chi Minh University of Technology, Vietnam, in 2006 and his M.S. degree from the École Nationale Supérieure de Mécanique et des Microtechniques de Besançon, France and the Hochschule Karlsruhe Technik und Wirtschaft, Germany in 2010. He is currently working towards the Ph.D degree at the École Nationale Supérieure d'Arts et Métiers, France. His research focuses on designing, modelling and controlling a system of multi-piezoelectric actuators to assist forging processes.

**Christophe Giraud-Audine** was born in Rabat (Morocco). He received his M.Eng. degree in mechanical engineering from the École Nationale Supérieure d'Arts et Métiers in 1992, and his Ph.D degree in electrical engineering from the Institut National Polytechnique de Toulouse in 1998. After two years spent as a Research Associate at the University of Sheffield, he joined an associate professor position at the École Nationale Supérieure d'Arts et Métiers. His current research focuses on the modelling and control of devices based on piezoelectric and shape memory alloys.

**Betty Lemaire-Semail** received her Ph. D degree in 1990 from the University of Paris XI, Orsay and habilitation degree in 1997 from the University of Lille 1. From 1990 to 1998, she was an assistant professor at the École Centrale de Lille and she is now a professor at the University of Lille 1. She is a member of the electrical engineering and power electronics laboratory of Lille (L2EP) and head of the research axis related to control of electrical systems. She has studied electromagnetic motors and her main field of interest now deals with the modelling and control of piezoelectric actuators for positioning and force feedback applications.

**Gabriel Abba** has joined the École Normale Supérieure de Cachan, France, in 1979, and received the “agrégation” of Ministry of Education in Electrical Engineering in 1982. He received the Doctorate degree in Electronics and Robotics from the University of Paris XI-Orsay, Paris, France, in 1986. Since 2004, he has been at The École Nationale d'Ingénieurs de Metz, where he is currently a Professor of Electrical and Computer Engineering. His research interests include development, modeling and control of robots, specially control of legged robots, visual servoing, manipulator control, design of robots and modelling and control of electromechanical actuators for industrial applications. He has made many contributions to robot dynamics and legged locomotion, and he has over 110 publications in Journals or Conferences.

**Régis Bigot** received his M.Eng. degree in mechanical engineering from the École Nationale Supérieure d'Arts et Métiers in 1992. In 1993 he obtained a master of sciences in Physics and Chemistry of Materials of University of Lille and his Ph.D degree in physical and metallurgy from the University of Lille in January 1996. After three years as technical teacher at Lille and Metz, he joined an associate professor position at the École Nationale Supérieure d'Arts et Métiers in September 1998. In September 2008, he becomes full professor in same institute. Since October 2011, he is director of Design, Manufacturing Engineering and Control Laboratory. His current research focuses on the manufacturing process (bulk forming, thixoforming, assembly, ...), integrated product and process design and CAPP.